Hydronephrosis with ureteritis developed in C57BL/6N mice carrying the congenic region derived from MRL/MpJ-type chromosome 11

Running Head: Ureteritis-hydronephrosis in MRL congenic mice

Authors: Osamu Ichii[1], Masataka Chihara[2], Shin-Hyo Lee[3], Teppei Nakamura[1,4], Saori Otsuka-Kanazawa[1], Taro Horino[5], Yaser Hosny Ali Elewa[1,6], and Yasuhiro Kon[1]

Affiliations:

[1]Laboratory of Anatomy, Department of Biomedical Sciences, Graduate School of Veterinary Medicine, Hokkaido University, Sapporo, Japan.

[2]R&D Department, Daiichi Sankyo healthcare Co., LTD., Tokyo, Japan.

[3]Department of Anatomy, Research Institute of Medical Science, Konkuk University School of Medicine, Seoul, Republic of Korea.

[4]Section of Biological Safety Research, Chitose Laboratory, Japan Food Research Laboratories, Chitose, Japan.

[5]Department of Endocrinology, Metabolism and Nephrology, Kochi Medical School, Kochi University, Nankoku, Japan.

[6]Department of Histology and Cytology, Faculty of Veterinary Medicine, Zagazig University, Zagazig, Egypt.

Corresponding Author

Dr. O. Ichii, D.V.M., Ph.D.,

Laboratory of Anatomy, Department of Biomedical Sciences, Graduate School of Veterinary Medicine, Hokkaido University, Kita18-Nishi 9, Kita-ku, Sapporo, Hokkaido 060-0818, Japan.

Tel.: +81-11-706-5188; Fax: +81-11-706-5189; E-mail: ichi-o@vetmed.hokudai.ac.jp

Abstract

Inbred MRL/MpJ mice show several unique phenotypes in tissue regeneration processes and the urogenital and immune systems. Clarifying the genetic and molecular bases of these phenotypes requires the analysis of their genetic susceptibility locus. Herein, hydronephrosis development was incidentally observed in MRL/MpJ-derived chromosome 11 (*D11Mit21-212*)-carrying C57BL/6N-based congenic mice, which developed bilateral or unilateral hydronephrosis in both males and females with 23.5% and 12.5% prevalence, respectively. Histopathologically, papillary malformations of the transitional epithelium in the pelvic-ureteric junction seemed to constrict the ureter luminal entrance. Characteristically, eosinophilic crystals were observed in the lumen of diseased ureters. These ureters were surrounded by infiltrating cells mainly composed of numerous $CD3^+$ T-cells and $B220^+$ B-cells. Furthermore, several Iba-1^+ macrophages, Gr-1^+ granulocytes, mast cells, and chitinase 3-like 3/Ym1 (an important inflammatory lectin)-positive cells were detected. Eosinophils also accumulated to these lesions in diseased ureters. Some B6.MRL-(*D11Mit21-D11Mit212*) mice had duplicated ureters. We determined >100 single nucleotide variants between C57BL/6N- and MRL/MpJ-type chromosome 11 congenic regions, which were associated with nonsynonymous substitution, frameshift, or stopgain of coding proteins. In conclusion, B6.MRL-(*D11Mit21-D11Mit212*) mice spontaneously developed hydronephrosis due to obstructive uropathy with inflammation. Thus, this mouse line would be useful for molecular pathological analysis of obstructive uropathy in experimental medicine.

Introduction

MRL/MpJ mice originate from C57BL/6J, C3H/HeDi, AKR/J, and LG/J strains. In particular, the mutant strain MRL/MpJ-*Fas*$^{lpr/lpr}$ is a representative model for autoimmune diseases [1]. In addition to autoimmune diseases, MRL/MpJ mice show some unique phenotypes related to wound healing such as accelerated ear punch closure and cardiomyocyte regeneration [2, 3]. We previously reported further unique characteristics in the urogenital organs of MRL/MpJ mice: i.e., increased apoptosis of meiotic spermatocytes [4], heat shock resistance of spermatocytes [5], existence of testicular oocytes in newborn males [6], development of ovarian cysts originating from the rete ovarii [7], appearance of numerous ovarian mast cells in neonatal females [8], and unique features of renal tissue repair after experimental kidney injuries [9].

These phenotypes were closely associated with the genetic background of MRL/MpJ mice, and we identified several susceptibility loci on their chromosomes (Chrs). From the genomic analysis, we revealed that the phenotype-related susceptibility loci in MRL/MpJ mice, and multiple loci on Chrs. 3, 4, 6, 11, and 14 interacted, resulting in the development of ovarian cysts [10]. Two loci on Chr. 8 were identified as susceptibility loci associated with the appearance of numerous ovarian mast cells in the neonatal period [11]. Furthermore, we demonstrated that the appearance of testicular oocytes is regulated by the genetic factors on Chrs. 15 and Y [12], and two significant quantitative trait loci (QTL) were located on Chrs. 1 and 11 for the heat shock resistance of spermatocytes in MRL/MpJ mice [13].

We previously generated C57BL/6N-based congenic mice carrying the telomeric region of MRL/MpJ-type Chr.1 (*D1Mit202-D1Mit403*) containing the susceptibility loci for testis- or autoimmune disease-associated phenotypes, and demonstrated that this congenic mice, named B6.MRL-(*D1Mit202-D1Mit403*), exhibited increased apoptosis of meiotic spermatocytes as well as severe autoimmune glomerulonephritis [14]. From the analysis of B6.MRL-(*D1Mit202-D1Mit403*) mice, exonuclease 1 on Chr. 1 was identified as a candidate gene of increased apoptosis of meiotic spermatocytes, and Fc receptor genes and interferon activated genes were considered as candidate genes for the development of glomerulonephritis in MRL/MpJ mice [15, 16]. We also examined the histopathological changes resulting from experimental cryptorchidism in the testes of the C57BL/6N-based congenic mice carrying the MRL/MpJ-derived loci responsible for heat-shock-resistant spermatocyte [5]. From the results of the congenic mice, we demonstrated that

MRL/MpJ-derived loci on Chrs. 1 and 11 regulated testicular heat sensitivity [5]. Thus, the congenic strain is a powerful tool to examine the pathological roles of phenotype-related susceptibility loci in inbred mice. All MRL/MpJ-derived susceptibility loci identified in our previous study were associated with immune or urogenital system-related phenotypes. Therefore, we speculated that congenic mice carrying these loci would show immune or urogenital system-related phenotypes. To examine the genetic function of the identified loci in MRL/MpJ-derived Chrs. and to discover candidate genes associated with immune or urogenital system-related phenotypes, we created several congenic strains carrying the genetic loci derived from MRL/MpJ [5, 14].

In this study, we report the development of hydronephrosis incidentally observed in C57BL/6N-based congenic mice carrying the MRL/MpJ-derived Chr. 11. These mice showed ureter abnormalities causing hydronephrosis due to obstructive uropathy with constant probability, and some mice presented with duplicated ureters. Furthermore, we identified more than 100 single nucleotide polymorphisms between C57BL/6N- and MRL/MpJ-type genome on the Chr. 11 congenic region, and they were associated with nonsynonymous substitution, frameshift, or stopgain of coding proteins. Thus, our congenic mice would be useful for the molecular pathological analysis of obstructive uropathy and developmental anomaly of the urinary organs in the field of experimental medicine.

Methods

Ethics statement

Animal experimentation was approved by the Institutional Animal Care and Use Committee, which was convened at the Graduate School of Veterinary Medicine, Hokkaido University (approval No. 13-0032). The investigators adhered to the Guide for the Care and Use of Laboratory Animals of Hokkaido University, Graduate School of Veterinary Medicine (approved by the Association for the Assessment and Accreditation of Laboratory Animal Care International).

C57BL/6N-based congenic mice carrying the MRL/MpJ-derived Chr. 11

Congenic mice were created as described previously from crossing C57BL/6N and MRL/MpJ mice purchased from Japan SLC, Inc. (Hamamatsu, Japan) [5]. Genomic DNA was prepared from the tail of each animal as described previously [14]. Briefly, these samples were incubated in lysis buffer and proteinase K, and then treated with two-phenol extraction. Genomic DNA was purified by ethanol precipitation, and congenic regions were examined by genotyping based on genome polymerase chain reaction for the microsatellite markers *D11Mit62*, *D11Mit21*, *D11Mit320*, *D11Mit212*, *D11Mit288*, *D11Mit199*, and *D11Mit48* (Fig. 1). The amplified samples were electrophoresed with 2% agarose gel and photographed under an ultraviolet lamp. The map positions of the microsatellite loci were based on information from the Mouse Genome Database (MGD) of The Jackson Laboratory (www.informatics.jax.org/).

Histopathological analysis

All mice were euthanized under deep anesthesia by exsanguination from the carotid arteries, and the spleens, kidneys, and ureters were immediately collected. Each tissue sample was fixed in 4% paraformaldehyde at 4°C for histopathological analysis. From fixed tissues, paraffin-embedded sections of kidneys and ureters were stained with hematoxylin-eosin, Masson’s trichrome, or periodic acid Schiff. A part of the ureter was fixed in 2.5% glutaraldehyde and 2% paraformaldehyde, dehydrated in a graded alcohol series, and embedded in Quetol 812. Semi-thin sections (500 nm) were stained with toluidine blue.

Immunostaining

For paraffin sections, immunohistochemistry for B220, CD3, Gr-1, Iba-1, and Ki67 was performed to detect the B-cells, pan T-cells, granulocytes, macrophages, and proliferating cells, respectively. The chitinase-like 3 (Chi3l3/Ym1) was also examined according to a previous study [17]. Details of the staining conditions and primary antibodies are listed in Table 1. In brief, the sections were deparaffinized, heated, and incubated with primary and secondary antibodies. For double staining, Alexa Fluor-conjugated antibodies were used as secondary antibodies. For immunohistochemistry, the color was developed by incubating the sections in a 3,3′-diaminobenzidine tetrahydrochloride-H_2O_2 solution. These stained sections were visualized with BZ-X710 all-in-one fluorescence microscope (Keyence, Osaka, Japan).

Deep sequencing

Kidney samples from C57BL/6N and MRL/MpJ mice were collected, and genomic DNA was isolated with DNeasy kit (Qiagen, Valencia, CA, USA). Exome-capture was performed using Sureselect XT Mouse All Exon kit (Agilent Technologies, Santa Clara, CA, USA). Whole Exome sequencing was performed with HiSeq2000 (Illumina, San Diego, CA, USA). UCSC mm10 (http://genome.ucsc.edu/) was used as the reference genome for alignment. The reads were mapped by BWA (version 0.5.9) (http://bio-bwa.sourceforge.net/). SNVs and small insertions/deletions were identified using SAMtools (ver.0.1.18) (http://samtools.sourceforge.net/).

Statistical analysis

The results are expressed as mean ± standard error (S.E.). Significant differences between 2 groups were analyzed by Mann-Whitney *U*-test with $P < 0.05$.

Results

C57BL/6N-based congenic mice carrying the MRL/MpJ-derived Chr. 11

Figure 1 shows the results of genotyping on Chr. 11 of C57BL/6N, congenic strain, and MRL/MpJ by using genomic DNA and microsatellite markers. In the congenic mice, *D11Mit21-212* (25.94 cM-54.34 cM; Chr. 11: 44,174,948–88,808,902 bp) were MRL/MpJ-type homozygous and the other regions were C57BL/6N-type homozygous. The mice were named B6.MRL-(*D11Mit21-D11Mit212*).

Incidence of hydronephrosis in B6.MRL-(D11Mit21-D11Mit212) mice

In the necropsy, B6.MRL-(*D11Mit21-D11Mit212*) mice developed bilateral or unilateral hydronephrosis showing urine retention to the renal pelvis (Fig. 2A and B). There was no apparent gross alteration in the other organs. The hydronephrotic kidney was approximately 2 folds heavier than healthy kidney (Fig. 2C). The incidence of hydronephrosis was higher in males (23.5%) compared to that of females (12.5%) at 11–15 weeks of ages, and these differences remained in males (25.0%) and females (13.0%) until 20–28 weeks of ages (Fig. 2D). The total incidence of hydronephrosis was higher in males (24.1%) compared to that in females (12.8%) (Fig. 2D). In males, the left kidney showed a slightly higher incidence rate than the right kidney, and bilateral hydronephrosis was found in several individuals (Fig. 2D). In females, a similar tendency was observed, but no bilateral hydronephrosis was observed in the mice examined (Fig. 2D). The ratio of spleen weight to body weight, an index of systemic immune condition, was significantly higher in animals developing hydronephrosis compared to healthy mice in B6.MRL-(*D11Mit21-D11Mit212*) mice (Fig. 2E).

Histopathology of hydronephrosis in B6.MRL-(D11Mit21-D11Mit212) mice

Hydronephrotic B6.MRL-(*D11Mit21-D11Mit212*) mice showed thinning renal cortices and enlarged renal pelvises containing retained urine (Fig. 3A and B). Furthermore, the mice showed papillary malformations of the transitional epithelium in the pelvic-ureteric junctions (Fig. 3A and C). Numerous cell infiltrations were observed around the mucosa of the proximal ureters (Fig. 3C). The healthy kidney showed the distinct connection between the renal pelvis and the ureter lumen (Fig. 3D). On the other hand, the hydronephrotic kidney showed a shortened renal papilla (Fig. 3E) and a constricted entrance of the ureter lumen by papillary malformations of the transitional epithelium (Fig.

3F). At the border between normal and abnormal transitional epithelium, the former showed a wrinkled surface but the latter showed hexagonal features (Fig. 3G-I).

Histopathology of the ureter in B6.MRL-(D11Mit21-D11Mit212) mice

Eosinophilic crystals were observed in the lumen of the diseased ureter surrounded by mononuclear cells, and eosinophilic materials were observed in the cytoplasm of transitional epithelial cells (Fig. 4A and B). Furthermore, mononuclear cells with non-segmented nuclei and eosinophilic granules as well as eosinophils infiltrated underneath the transitional epithelium (Fig. 4B). Gland-like structures containing dead mononuclear cells, granulocytes, dropped transitional epithelial cells, and eosinophilic crystals were observed outside the muscular layer (Fig. 4C). Severe cell infiltrations from the lamina propria to the adventitia and these lesions were also noted (Fig. 4C). The Chi3l3/Ym1 protein, a lectin overexpressed in the ureter of hydronephrosis mice [17] and associated with inflammation, transitional epithelium adenoma, and the formation of eosinophilic crystals [18] was observed in the cytoplasm of infiltrating cells, apical portion of transitional epithelial cells, and cell debris or crystal structures of the ureter lumen (Fig. 4D). In the pelvic-ureteral junction of hydronephrotic mice, Ki67-positive proliferative cells were scarcely observed in the ureteral transitional epithelium (Fig. 4E), but were abundant in the central position of cell infiltration lesions (Fig. 4F). The distal ureter also showed an increase in the interstitium and cell infiltrations from the lamina propria to the adventitia (Fig. 4G). The cell infiltration was composed of numerous CD3-positive T-cells, B220-positive B-cells, several Gr-1-positive granulocytes, and Iba-1-positive macrophages (Fig. 4H and I). In addition, numerous eosinophil infiltrations were observed in some regions (Fig. 4J). Along the whole length of the diseased ureters, fibrotic features were observed from the lamina propria to the adventitia (Fig. 4K).

Incidental duplicated ureters in B6.MRL-(D11Mit21-D11Mit212) mice

We found duplicated ureters in two of all the examined B6.MRL-(*D11Mit21-D11Mit212*) mice (Fig. 5). These ureters ran parallel to each other (Fig. 5A and B), had a common serosa (Fig. 5B), and one of them showed stenosis features containing cell debris (Fig. 5A-C). These cell debris were composed of dropped epithelial cells and crystals (Fig. 5D). Several mast cells, showing metachromasia in toluidine blue stain, were also observed around the ureters (Fig. 5D).

202

203 *SNV between C57BL/6N- and MRL/MpJ-type genome on congenic region in*
204 *B6.MRL-(D11Mit21-D11Mit212) mice*

205 We compared the SNV between C57BL/6N- and MRL/MpJ-type genomes on the congenic region
206 in B6.MRL-(*D11Mit21-D11Mit212*) mice by Whole Exome sequencing. As a result, over 100 of
207 nonsynonymous single nucleotide variants (SNVs) and 12 variants associated with frameshift or
208 stopgain such as the olfactory receptor family, FAT atypical cadherin 2 (*Fat2*), butyrophilin-like 10
209 (*Btnl10*), obscurin, cytoskeletal calmodulin and titin-interacting RhoGEF (*Obscn*), IBA57 homolog,
210 iron-sulfur cluster assembly (*Iba57*), myosin XV (*Myo15*), and tripartite motif-containing 16 (*Trim16*),
211 were detected in MRL/MpJ-type Chr. 11 when compared to C57BL/6N (Table 1).

212

Discussion and Conclusion

Pelvic-ureteric junction obstruction is a common cause of human hydronephrosis and results from the narrowing of the renal pelvis and ureter [19, 20]. In experimental medicine, the hydronephrosis model is usually created by an ureteric obstruction operation, and few studies reported hydronephrosis in specific-gene modification models such as the promyelocytic leukemia (*PML*)/retinoic acid receptor alpha (*RARA*), a chimeric gene of *PML* and *RARA* knock-in mice, and interleukin (*Il9*)-overexpressing mice [18, 21]. Because the spontaneous model of hydronephrosis due to obstructive uropathy without gene modification is scarce, the details of its pathogenesis are still unclear.

In this study, we newly discovered the spontaneous development of hydronephrosis in congenic mice carrying MRL/MpJ-type Chr.11 (*D11Mit21-212*) and C57BL/6N-type genetic background. From the histopathological features, stenosis of the pelvic-ureteric junction due to papillary malformations of the transitional epithelium seemed to contribute to the development of hydronephrosis. Interestingly, their histopathological features were similar to the hydronephrosis observed in *PML/PARA* knock-in mice and *Il9*-overexpressing mice [18, 21] as well as the F2 generation between C57BL/6 and DBA/2 mice as reported in our previous study [17]. IL-9 is a regulator of Th2 effector cytokines, and *Il9*-overexpressing mice developed T-cell lymphoma [21]. *PML*/*RARA* induces myeloproliferative syndrome, and *PML/RARA* knock-in mice developed acute myeloid leukemia [18]. Although (C57BL/6 × DBA/2) F2 mice [17] as well as B6.MRL-(*D11Mit21-D11Mit212*) mice did not show any systemic immune disorders, both mice commonly manifested lymphocyte infiltrations in the diseased ureters. In fact, the spleen weights increased in B6.MRL-(*D11Mit21-D11Mit212*) mice developing hydronephrosis, but representative lesions associated with autoimmune disease such as glomerulonephritis were not observed.

Characteristically, large granular leukocytes and eosinophils infiltrated the ureters of B6.MRL-(*D11Mit21-D11Mit212*) mice. These cells were also found in *Il9*-overexpressing mice, *PML/PARA* knock-in mice, and (C57BL/6 × DBA/2) F2 mice [17, 18, 21]. Compared to the incidence of hydronephrosis in (C57BL/6 × DBA/2) F2 mice (5–7%) [21], B6.MRL-(*D11Mit21-D11Mit212*) mice showed a higher incidence of hydronephrosis (23.5% in males and 12.5% in females). Although there are several differences in the pathological features among hydronephrotic models, genetic factors

derived from MRL/MpJ-type Chr. 11 or C57BL/6N-type genome and/or their interactions contribute to the development of hydronephrosis in B6.MRL-(*D11Mit21-D11Mit212*) mice, in particular due to the alteration of immune conditions in the urinary system. Furthermore, because the development of hydronephrosis was not observed in the F1 generation between C57BL/6 mice and DBA/2 mice in our previous study [21], homogenous genetic factors may have crucial roles in the development of hydronephrosis.

Urinary tract obstruction could be caused by ureteral stones, urothelial tumors, and infectious or idiopathic inflammation in humans. The pathological features of the ureters in B6.MRL-(*D11Mit21-D11Mit212*) mice partially overlapped with human idiopathic ureteritis diagnosed as inflammatory pseudotumor (IPT) of the ureter, idiopathic segmental ureteritis (ISU), idiopathic retroperitoneal fibrosis (IRF) involving the ureters, or eosinophilic ureteritis [19, 22-25]. The latter 2 diseases are accompanied by peritoneal fibrosis and systemic immunological changes such as atopy, respectively [19, 22, 23], but these symptoms were not observed in the diseased B6.MRL-(*D11Mit21-D11Mit212*) mice. Similar to the B6.MRL-(*D11Mit21-D11Mit212*) ureters, the ureters in IPT and ISU show infiltrations of lymphoplasma cells and eosinophils as well as sclerotic fibrosis [24, 25] and some cases of IPT show ureteric malformations [25]. Furthermore, male infants show a greater prevalence of hydronephrosis compared to females in humans [26, 27], and this sex-related tendency resembles the hydronephrosis observed in the B6.MRL-(*D11Mit21-D11Mit212*) mice. This is an important consideration because obstructive uropathies are diagnosed in aging human populations. However, no age-related tendency was observed in the development of hydronephrosis in the B6.MRL-(*D11Mit21-D11Mit212*) mice (Fig. 1D).

A previous study reported the spontaneous development of ureteric obstructions caused by polyploid adenomas locating from the renal pelvis to the ureter with severe cell infiltration and the appearance of Chil3l3/Ym1-positive crystals in acute myeloid leukemia o*f PML/PARA* knock-in mice [18]. Furthermore, in the hydronephrotic ureters of (C57BL/6 × DBA/2) F2 mice, comprehensive gene expression analysis revealed that the factors regulating ureteric local inflammation, the *Chil3l3* gene in particular, showed ectopic and remarkably elevated expression [17]. Interestingly, Chil3l3/Ym1 was also detected in the cytoplasm of infiltrating cells, apical portion of transitional epithelial cells, and cell debris or crystal structures of ureter lumen in B6.MRL-(*D11Mit21-D11Mit212*) mice. Chil3l3/Ym1 is an

endogenous lectin, widely distributed in normal mammalian bodies, and expressed transiently in early myeloid precursor cells of hematopoietic tissues: initially in the yolk sac and subsequently in the fetal liver, spleen, and bone marrow [18, 28, 29-30]. In addition, Chil3l3/Ym1 promotes Th2 cytokine expression in allergic responses, suggesting an important role of Chil3l3/Ym1 in hematopoiesis as well as inflammation [31]. Therefore, the appearance of Chil3l3/Ym1 expressing cells might reflect altered local immune conditions in the ureters of B6.MRL-(*D11Mit21-D11Mit212*) mice.

Additionally, comprehensive gene expression analysis of the hydronephrotic ureters of (C57BL/6 × DBA/2) F2 mice revealed that the B-cell functions such as B-cell activation, the B-cell receptor signaling pathway, and B-cell proliferation were important for the pathogenesis in this disease based on gene ontology and expression analyses [17]. Furthermore, inflammatory mediators such as the family members of mast cell protease, matrix metalloproteinase, or chemokine (C-C motif) ligand were remarkably upregulated in the diseased ureters compared to that in the healthy ureters in hydronephrotic (C57BL/6 × DBA/2) F2 mice [17]. Numerous B-cell infiltrations were also observed in the ureters of B6.MRL-(*D11Mit21-D11Mit212*) mice developing hydronephrosis. Therefore, in future studies, the determination of specific cell subsets, in particular those of B-cells, with the analysis of inflammatory mediator producing capacities would be needed to better understand the pathogenesis of ureteritis-hydronephrosis developing mice.

The phenotype of heat shock resistance of the spermatocytes in MRL/MpJ is closely associated with Chr. 11 (*D11Mit21-212*) [5]. However, there seemed to be no significant association between this testicular phenotype and the hydronephrosis detected in B6.MRL-(*D11Mit21-D11Mit212*) mice. Interestingly, a few B6.MRL-(*D11Mit21-D11Mit212*) mice developed duplicated ureters as previously reported in humans and dogs [32, 33], and this malformation could cause hydronephrosis due to urinary tract obstruction. Therefore, the molecular pathogenesis of hydronephrosis in B6.MRL-(*D11Mit21-D11Mit212*) mice might involve immune functions as well as urinary tract development.

To identify the SNV between the C57BL/6N- and MRL/MpJ-type genome on the congenic region in B6.MRL-(*D11Mit21-D11Mit212*) mice, we performed Whole Exome sequencing and identified over 100 nonsynonymous SNVs. Interestingly, 12 variants associated with frameshift or stopgain such as the

Olfr family, *Fat2*, *Btnl10*, *Obscn*, *Iba57*, *Myo15*, and *Trim16* were identified between MRL/MpJ-type Chr. 11 and C57BL/6N. However, there are no report about the relationship between these genes and the urinary tract system. Mice carrying the null-mutated Forkhead box C1 (*Foxc1*) gene frequently develop congenital anomalies of the kidney and urinary tract such as duplicated ureters [34], but this gene is coded on Chr. 13. The coding genes of RARA, PML, and IL-9, hydronephrosis-associated molecules, were not located on Chr. 11 *(D11Mit21-212*). Thus, the SNV identified in this study might be useful to elucidate the novel pathogenesis associated with the immune system and the development of urinary tract system in future studies. In addition, we should consider the contribution of the C57BL/6N-genetic background, because mice carrying the C57BL/6N-type genetic background have been shown to develop eosinophilic macrophage pneumonia with the appearance of eosinophilic crystals [35, 36]. Large eosinophilic crystals were also observed in the lumen of ureters in B6.MRL-(*D11Mit21-D11Mit212*) mice, and similar crystals composed of endogenous lectin were observed in several diseases with severe eosinophil infiltration such as parasitosis and asthma [37].

In conclusion, B6.MRL-(*D11Mit21-D11Mit212*) mice spontaneously developed hydronephrosis due to obstructive uropathy with inflammation. Therefore, this animal model would be useful for the molecular pathological analysis of obstructive uropathy and developmental anomaly of the urinary organs.

Acknowledgments

NA

Funding

This work was partially supported by JSPS KAKENHI, grant # 15K14873 and 15H05634.

Declaration of Interest

This manuscript has not been published or presented elsewhere in part or in entirety, and is not under consideration by another journal. All authors have approved the manuscript and agree with submission to this journal. There are no conflicts of interest to declare.

References

1. Otani, Y., O. Ichii, S. Otsuka-Kanazawa, M. Chihara, T. Nakamura, and Y. Kon. 2015. MRL/MpJ-Fas (lpr) mice show abnormalities in ovarian function and morphology with the progression of autoimmune disease. *Autoimmunity* 48:402–411.
2. Leferovich, J. M., K. Bedelbaeva, S. Samulewicz, X. M. Zhang, D. Zwas, E. B. Lankford, and E. Heber-Katz. 2001. Heart regeneration in adult MRL mice. *Proc. Natl. Acad. Sci. USA* 98:9830–9835.
3. Rajnoch, C., S. Ferguson, A. D. Metcalfe, S. E. Herrick, H. S. Willis, and M. W. Ferguson. 2003. Author information Regeneration of the ear after wounding in different mouse strains is dependent on the severity of wound trauma. *Dev. Dyn.* 226:388–397.
4. Otsuka, S., Y. Namiki, O. Ichii, Y. Hashimoto, N. Sasaki, D. Endoh, and Y. Kon. 2010. Analysis of factors decreasing testis weight in MRL mice. *Mamm. Genome* 21:153–161.
5. Chihara, M., T. Nakamura, S. Otsuka-Kanazawa, O. Ichii, Y. H. Elewa, and Y. Kon. 2015. Genetic factors derived from the MRL/MpJ mouse function to maintain the integrity of spermatogenesis after heat exposure. *Andrology* 3: 991–999.
6. Otsuka-Kanazawa, S., O. Ichii, and Y. Kon. 2015. Testicular oocytes in MRL/MpJ mice possess similar morphological, genetic, and functional characteristics to ovarian oocytes. *Mech. Dev.* 137: 23–32.
7. Lee, S.H., O. Ichii, S. Otsuka, Y. H. Elewa, Y. Namiki, Y. Hashimoto, and Y. Kon. 2011. Ovarian cysts in MRL/MpJ mice are derived from the extraovarian rete: a developmental study. *J. Anat.* 219: 743–755.
8. Nakamura, T., S. Otsuka, O. Ichii, Y. Sakata, K. Nagasaki, Y. Hashimoto, and Y. Kon. 2013. Relationship between numerous mast cells and early follicular development in neonatal MRL/MpJ mouse ovaries. *PLoS One* 8:e77246.

9. Shiozuru, D., O. Ichii, J. Kimura, T. Nakamura, Y. H. Elewa, S. Otsuka-Kanazawa, and Y. Kon. 2016. MRL/MpJ mice show unique pathological features after experimental kidney injury. *Histol. Histopathol.* 31:189–204.

10. Lee S.H., O. Ichii, S. Otsuka, Y. Hashimoto, and Y. Kon. 2010. Quantitative trait locus analysis of ovarian cysts derived from rete ovarii in MRL/MpJ mice. *Mamm. Genome* 21: 162–171.

11. Nakamura, T., Y. Sakata, S. Otsuka-Kanazawa, O. Ichii, M. Chihara, K. Nagasaki, Y. Namiki, and Y. Kon. 2014. Genomic analysis of the appearance of ovarian mast cells in neonatal MRL/MpJ mice. *PLoS One* 9:e100617.

12. Otsuka, S., O. Ichii, Y. Namiki, N. Sasaki, Y. Hashimoto, and Y. Kon. 2012. Genomic analysis of the appearance of testicular oocytes in MRL/MpJ mice. *Mamm. Genome* 23:741–748.

13. Namiki, Y., Y. Kon, K. Kazusa, A. Asano, N. Sasaki, and T. Agui. 2005. Quantitative trait loci analysis of heat stress resistance of spermatocytes in the MRL/MpJ mouse. *Mamm. Genome* 16:96–102.

14. Ichii, O., A. Konno, N. Sasaki, D. Endoh, Y. Hashimoto, and Y. Kon. Autoimmune glomerulonephritis induced in congenic mouse strain carrying telomeric region of chromosome 1 derived from MRL/MpJ. *Histol. Histopathol.* 23 : 411–422.

15. Ichii, O., A. Konno, N. Sasaki, D. Endoh, Y. Hashimoto, and Y. Kon. 2008. Altered balance of inhibitory and active Fc gamma receptors in murine autoimmune glomerulonephritis. *Kidney Int.* 74:339–347.

16. Ichii, O., A. Kamikawa, S. Otsuka, Y. Hashimoto, N. Sasaki, D. Endoh, and Y. Kon. 2010. Overexpression of interferon-activated gene 202 (Ifi202) correlates with the progression of autoimmune glomerulonephritis associated with the MRL chromosome 1. *Lupus* 19: 897–905.

17. Ichii, O, S. Otsuka, Y. Namiki, Y. Hashimoto, and Y. Kon. 2011. Molecular pathology of murine ureteritis causing obstructive uropathy with hydronephrosis. *PLoS One* 6 :e27783.

18. Marchesi, F., S. Minucci, P. G. Pelicci, A. Gobbi, and E. Scanziani. 2006. Immunohistochemical detection of Ym1/Ym2 chitinase-like lectins associated with hyalinosis and polypoid adenomas of the transitional epithelium in a mouse with acute myeloid leukemia. *Vet. Pathol.* 43:773–776.

19. Spark, R. P., D. M. Gleason, C. D. DeBenedetti, and J. H. Gigax. 1991. Is eosinophilic ureteritis an entity? 2 case reports and review. *J. Urol.* 145:1256–1260.

20. Elder, J. S. 1997. Antenatal hydronephrosis. Fetal and neonatal management. *Pediatr. Clin. North Am.* 44: 1299–1321.

21. Lauder, A.J., H. E. Jolin, P. Smith, J. G. van den Berg, A. Jones, W. Wisden, K. G. Smith, A. Dasvarma, P. G. Fallon, and A. N. McKenzie. 2004. Lymphomagenesis, hydronephrosis, and autoantibodies result from dysregulation of IL-9 and are differentially dependent on Th2 cytokines. *J. Immunol.* 173:113–122.

22. Sergeant, G., K. Slabbaert, and P. Werbrouck. 2004. Recurrent flank pain caused by eosinophilic ureteritis mimicking urinary stone disease: a case report. *Int. Urol. Nephrol.* **36**:23–25.

23. Corradi, D., R. Maestri, A. Palmisano, S. Bosio, P. Greco, L. Manenti, S. Ferretti, R. Cobelli, G. Moroni, A. P. Dei Tos, C. Buzio, and A. Vaglio. 2007. Idiopathic retroperitoneal fibrosis: clinicopathologic features and differential diagnosis. *Kidney Int.* 72: 742–753.

24. Joo, M., S. H. Chang, H. Kim, K. C. Lee, and J. Y. Ro. 2010. Idiopathic segmental ureteritis, misdiagnosed as ureteral cancer preoperatively: a case report with literature review. *Pathol. Int.* 60: 779–783.

25. Kim, S. A., S. R. Lee, J. Huh, S. S. Shen, J. Y. Ro. 2011. IgG4-associated inflammatory pseudotumor of ureter: clinicopathologic and immunohistochemical study of 3 cases. *Hum. Pathol.* 42:1178–1184.

26. Yeung, C. K., M. L. Godley, H. K. Dhillon, I. Gordon, P. G. Duffy. 1997. The characteristics of primary vesico-ureteric reflux in male and female infants with pre-natal hydronephrosis. *Br. J. Urol.*

398 80:319–327.
399 27. Sherer, D. M. 2000. Is fetal hydronephrosis overdiagnosed? *Ultrasound. Obstet. Gynecol.* 16:601–
400 606.
401 28. Ward, J. M., M. Yoon, M. R. Anver, D. C. Haines, G. Kudo, F. J. Gonzalez, and S. Kimura. 2001.
402 Hyalinosis and Ym1/Ym2 gene expression in the stomach and respiratory tract of 129S4/SvJae and
403 wild-type and CYP1A2-null B6, 129 mice. *Am. J. Pathol.* 158:323–332.
404 29. Marchesi, F., S. V. Monestiroli, M. Capillo, A. Gobbi, S. Minucci, P. G. Pelicci, and E. Scanziani.
405 2003. Eosinophilic crystals as a distinctive morphologic feature of a hyaline droplet nephropathy in
406 a mouse model of acute myelogenous leukaemia. *J. Vet. Med. A. Physiol. Pathol. Clin. Med.*
407 50:103–107.
408 30. Nio, J., W. Fujimoto, A. Konno, Y. Kon, M. Owhashi. 2004. Cellular expression of murine Ym1
409 and Ym2, chitinase family proteins, as revealed by in situ hybridization and immunohistochemistry.
410 *Histochem. Cell Biol.* 121:473–482.
411 31. Cai, Y., R.K. Kumar, J. Zhou, P. S. Foster, and D. C. Webb. 2009. Ym1/2 promotes Th2 cytokine
412 expression by inhibiting 12/15(S)-lipoxygenase: identification of a novel pathway for regulating
413 allergic inflammation. *J. Immunol.* 182: 5393–5399.
414 32. Gonzalez, F., D. A. Canning, G. Hyun, and P. Casale. 2006. Lower pole pelvi-ureteric junction
415 obstruction in duplicated collecting systems. *BJU Int.* 97: 161–165.
416 33. Newman, M., and B. Landon. 2014. Surgical treatment of a duplicated and ectopic ureter in a dog.
417 *J. Small Anim. Pract.* 55:475–478.
418 34. Kume, T., K. Deng, B. L. Hogan. 2000. Murine forkhead/winged helix genes Foxc1 (Mf1) and
419 Foxc2 (Mfh1) are required for the early organogenesis of the kidney and urinary tract.
420 *Development* 127 :1387–1395.
421 35. Murray, A. B., and A. Luz. 1990. Acidophilic macrophage pneumonia in laboratory mice. *Vet.*

Pathol. 27:274–281.

36. Hoenerhoff, M. J., M. F. Starost, and J. M. Ward. 2006. Eosinophilic crystalline pneumonia as a major cause of death in 129S4/SvJae mice. *Vet. Pathol*. 43 :682–688.

37. Lin, T. A., G. Kourteva, H. Hilton, H. Li, and N. S. Tare. 2010. The mRNA level of Charcot-Leyden crystal protein/galectin-10 is a marker for CRTH2 activation in human whole blood in vitro. *Biomarkers* 15: 646–654.

Figure Legends

Fig. 1. Chr. 11 of B6.MRL-(*D11Mit21-D11Mit212*) mice.

Genotyping genomic DNA using microsatellite markers (left panels). The polymorphisms between the strains are detected as size differences in the PCR products. Schematic representation (right panel). In B6.MRL-(*D11Mit21-D11Mit212*) mice, *D11Mit62* (5.78 cM) and *D11Mit288-48* (58.90–82.96 cM) were C57BL/6N types, and *D11Mit21-320* (25.94–54.34 cM) was MRL/MpJ type.

Fig. 2. Hydronephrosis in B6.MRL-(*D11Mit21-D11Mit212*) mice.

(**A, B**) Gross anatomical features of hydronephrosis in B6.MRL-(*D11Mit21-D11Mit212*) mice. Unilateral hydronephrosis showing urine retention to the renal pelvis are observed. Arrows indicate ureter hypertrophy in proximal portions.

(**C**) Relative increase of weights in the hydronephrotic kidneys of B6.MRL-(*D11Mit21-D11Mit212*) mice. Values = mean ± S.E., n > 4.

(**D**) The incidence of hydronephrosis in B6.MRL-(*D11Mit21-D11Mit212*) mice. The number of analyzed mice is described in the graphs. N.D.: not detected.

(**E**) Ratio of spleen weight to body weight in B6.MRL-(*D11Mit21-D11Mit212*) mice with or without the development of hydronephrosis. Male and female individuals are included at 11–28 weeks of age. Values = mean ± S.E. *: significant difference with normal group.

Fig. 3. Histopathology of hydronephrosis in B6.MRL-(*D11Mit21-D11Mit212*) mice

(**A-C**) Histopathological features of the kidney and ureter (UR) in hydronephrotic B6.MRL-(*D11Mit21-D11Mit212*) mice assessed by hematoxylin and eosin staining. Thinning renal cortex (CO) and enlarged renal pelvis (RP) are observed (A and B). Papillary malformations of the transitional epithelium (arrows) are observed in the pelvic-ureteric junction (C). Numerous cell infiltrations are also observed around the mucosa of the proximal ureter (C, left side).

(**D-I**) Surface structures of the lumens in RP and UR of B6.MRL-(*D11Mit21-D11Mit212*) mice assessed by SEM. Smooth transition of RP mucosa to UR mucosa (D). AT: adipose tissue. Kid: kidney. The renal

papilla is shortened (arrow) and RP is enlarged (E). Papillary malformations of the transitional epithelium constricted the entrance of the ureter lumen (F, asterisk). Border between normal (dagger) and abnormal (asterisk) transitional epithelium (G). In these positions, the former shows a wrinkled surface (arrows), but the latter shows hexagonal features (arrowheads) (H and I).

Fig. 4. Histopathology of the ureter in B6.MRL-(*D11Mit21-D11Mit212*) mice.

(**A-K**) Histopathological features of the ureters in hydronephrotic B6.MRL-(*D11Mit21-D11Mit212*) mice. Hematoxylin and eosin staining (A-C, G, and J). Immunohistochemistry (D-F). Immunofluorescence (H and I). Masson's trichrome staining (K). Eosinophilic crystals and eosinophilic materials are observed in the lumen (Lu) of the diseased ureter surrounded by mononuclear cells (A, arrow) and in the cytoplasm of transitional epithelial cells (A, arrowheads). Eosinophilic materials are clearly observed in the cytoplasm of transitional epithelial cells (B). Mononuclear cells with non-segmented nuclei and eosinophilic granules (B, arrow) and eosinophils (B, arrowheads) infiltrated the transitional epithelium. Gland-like structures containing dead mononuclear cells, granulocytes, dropped transitional epithelial cells, and eosinophilic crystals are observed outside of the muscular layer (C, arrow). Severe cell infiltrations are noted (C) Chi3l3/Ym1-positive reactions are observed in the cytoplasm of infiltrating cells (D, arrows), apical portion of transitional epithelial cells (D), and cell debris or crystal structures (D, arrowheads and inset) of the ureter lumen. Ki67-positive proliferative cells are scarcely observed in the ureteral transitional epithelium (E), but are present in the central position of cell infiltration lesions (F, arrow). The distal ureter shows increased interstitium and cell infiltrations (G). The cell infiltrations are composed of numerous CD3-positive T-cells (H, red), B220-positive B-cells (I, green), several Gr-1-positive granulocytes (H, green, arrow), and Iba-1-positive macrophages (I, red). Numerous eosinophil infiltrations are observed in some regions (J). Along the whole length of the diseased ureter, fibrotic features (blue) are observed from the lamina propria to the adventitia (K).

(**L**) Histopathological features of the renal cortex in hydronephrotic B6.MRL-(*D11Mit21-D11Mit212*) mice at 20 weeks of age assessed by periodic acid Schiff staining. There is no glomerular lesion (arrows). Asterisks indicate dilated renal tubules.

Fig. 5. Duplicated ureters in B6.MRL-(*D11Mit21-D11Mit212*) mice.

Histopathological features of duplicated ureters are incidentally observed in some B6.MRL-(*D11Mit21-D11Mit212*) mice. Hematoxylin and eosin staining (A). Toluidine blue staining (B-D). Duplicated ureters run parallel to each other (A). Duplicated ureters have common serosa (B). One of the ureters shows stenosis features containing cell debris (A, left side; B, upper one; C, lower one). These cell debris are composed of dropped epithelial cells and crystals (C and D). Several mast cells showing metachromasia are observed around the ureters (D, arrow). Lu: lumen.

Table 1. Antibodies, working dilutions, and methods for antigen retrieval.

Antibody	Source	Dilution	Antigen retrieval	Heating condition
Rabbit anti-Ki67		1:150	10 mM Citrate buffer (pH 6.0)	105°C, 20 min
Rat anti-Chi3l3/Ym1	R and D system (Minneapolis, MN, USA)	1:400	20 mM Tris-HCl (pH 9.0)	105°C, 20 min
Rabbit anti-Iba1	Wako (Osaka, Japan)	1:1000	20 mM Tris-HCl (pH 9.0)	37°C, 5 min
Rat anti-Gr1	R and D system	1:400	0.1% pepsin/ 0.2 N HCl	37°C, 5 min
Rat anti-B220	Cedarlane (Ontario, Canada)	1:800	20 mM Tris-HCl (pH 9.0)	105°C, 20 min
Rabbit anti-CD3	Nichirei (Tokyo, Japan)	1:200	0.1% pepsin/ 0.2 N HCl	105°C, 20 min

Table 2. Summary of SNV determined by Whole Exome sequencing between C57BL6N and MRL/MpJ in Chr. 11 congenic regions.

Gene	Change description	Start	End	C57BL/6N	MRL/MpJ	Homo/Hetero	SNP quality
			Nonsynonymous substitution				
Havcr2	nonsynonymous_SNV6	46456267	46456267	A	G	hom	153
Gm12169	nonsynonymous_SNV2	46528416	46528416	C	G	hom	186
Gm12171	nonsynonymous_SNV1	46548446	46548446	C	T	hom	160
BC053393	nonsynonymous_SNV2	46577230	46577230	A	G	hom	222
Havcr1	nonsynonymous_SNV3	46752306	46752306	G	A	hom	222
Timd4	nonsynonymous_SNV2	46810846	46810846	C	T	hom	222
Maml1	nonsynonymous_SNV1	50263308	50263308	T	A	hom	59
Csf2	nonsynonymous_SNV1	54247598	54247598	C	A	hom	220
Il3	nonsynonymous_SNV4	54266977	54266977	T	C	hom	150
4930404A10Rik	nonsynonymous_SNV1	54370917	54370917	G	A	hom	212
Tnip1	nonsynonymous_SNV1	54940825	54940825	C	G	hom	140
Anxa6	nonsynonymous_SNV3	54983317	54983317	T	A	hom	214
Fat2	nonsynonymous_SNV2	55262499	55262499	G	A	hom	221
Nmur2	nonsynonymous_SNV1	56040278	56040278	T	C	hom	222
Fam114a2	nonsynonymous_SNV5	57484032	57484032	A	G	hom	167
Mfap3	nonsynonymous_SNV2	57528040	57528040	A	T	hom	198
Galnt10	nonsynonymous_SNV1	57765688	57765688	G	A	hom	222
Larp1	nonsynonymous_SNV1	58042340	58042340	G	A	hom	222
Gemin5	nonsynonymous_SNV6	58122289	58122289	C	G	hom	222
Mrpl22	nonsynonymous_SNV1	58171695	58171695	G	A	hom	222
Gm12250	nonsynonymous_SNV3	58187802	58187802	T	C	hom	222
Igtp	nonsynonymous_SNV4	58206343	58206343	T	G	hom	222
Irgm2	nonsynonymous_SNV9	58219513	58219513	T	A	hom	195
Zfp692	nonsynonymous_SNV2	58309033	58309033	G	T	hom	222
Lypd8	nonsynonymous_SNV6	58382775	58382775	T	C	hom	222
1810065E05Rik	nonsynonymous_SNV3	58422201	58422201	C	T	hom	170
Gm12253	nonsynonymous_SNV6	58434541	58434541	G	C	hom	222
Olfr332	nonsynonymous_SNV2	58490297	58490297	C	T	hom	222
Olfr331	nonsynonymous_SNV11	58501648	58501648	T	C	hom	222
Olfr329-ps	nonsynonymous_SNV1	58543446	58543446	G	T	hom	222
Olfr328	nonsynonymous_SNV3	58551561	58551561	T	C	hom	152
Olfr224	nonsynonymous_SNV2	58566562	58566562	G	A	hom	222
Olfr325	nonsynonymous_SNV4	58580931	58580931	T	C	hom	221
Olfr324	nonsynonymous_SNV4	58597518	58597518	A	C	hom	222
2210407C18Rik	nonsynonymous_SNV3	58608509	58608509	G	A	hom	32.3
Olfr323	nonsynonymous_SNV3	58625762	58625762	G	A	hom	156
Trim58	nonsynonymous_SNV3	58640858	58640858	C	A	hom	222
Olfr322	nonsynonymous_SNV3	58665691	58665691	T	C	hom	102
Olfr320	nonsynonymous_SNV8	58683932	58683932	G	T	hom	157
Olfr319	nonsynonymous_SNV2	58701958	58701958	A	C	hom	222
Olfr318	nonsynonymous_SNV2	58720458	58720458	G	A	het	107
Olfr317	nonsynonymous_SNV2	58732215	58732215	T	C	hom	199
Olfr316	nonsynonymous_SNV7	58757967	58757967	G	A	hom	183
Olfr313	nonsynonymous_SNV5	58817061	58817061	A	G	hom	222
Olfr311	nonsynonymous_SNV2	58841119	58841119	G	T	hom	222
2810021J22Rik	nonsynonymous_SNV6	58878844	58878844	A	G	hom	218

Zfp39	nonsynonymous_SNV7	58889867	58889867	C	T	hom	112
Trim17	nonsynonymous_SNV1	58970446	58970446	A	G	hom	221
Obscn	nonsynonymous_SNV54	59000884	59000884	C	T	hom	196
Iba57	nonsynonymous_SNV2	59161555	59161555	T	C	hom	222
Gjc2	nonsynonymous_SNV2	59176433	59176433	T	C	hom	199
Mrpl55	nonsynonymous_SNV1	59204589	59204589	A	T	hom	203
Prss38	nonsynonymous_SNV2	59375551	59375551	G	T	hom	187
Jmjd4	nonsynonymous_SNV3	59450788	59450788	A	G	hom	154
Zfp867	nonsynonymous_SNV2	59463105	59463105	A	G	hom	33.3
Zkscan17	nonsynonymous_SNV4	59487650	59487650	C	T	hom	222
Nlrp3	nonsynonymous_SNV2	59555785	59555785	G	A	hom	222
Olfr223	nonsynonymous_SNV1	59589934	59589934	G	T	hom	219
Olfr225	nonsynonymous_SNV7	59613209	59613209	A	G	hom	222
Mprip	nonsynonymous_SNV2	59749606	59749606	G	A	hom	222
Pemt	nonsynonymous_SNV1	60031784	60031784	T	C	hom	222
Rai1	nonsynonymous_SNV5	60185857	60185857	A	G	hom	212
Srebf1	nonsynonymous_SNV1	60200146	60200146	T	C	hom	222
Lrrc48	nonsynonymous_SNV5	60364958	60364958	G	A	hom	191
Myo15	nonsynonymous_SNV7	60477716	60477716	A	G	hom	189
Flii	nonsynonymous_SNV2	60716732	60716732	T	C	hom	222
Mief2	nonsynonymous_SNV3	60730943	60730943	C	T	hom	222
Top3a	nonsynonymous_SNV5	60742577	60742577	G	A	hom	193
Smcr8	nonsynonymous_SNV3	60779106	60779106	T	C	hom	222
Kcnj12	nonsynonymous_SNV3	61066752	61066752	T	C	hom	144
Zfp287	nonsynonymous_SNV2	62713807	62713807	C	T	hom	222
Zfp286	nonsynonymous_SNV4	62780692	62780692	T	C	hom	92
Trim16	nonsynonymous_SNV4	62820602	62820602	C	T	hom	222
Fbxw10	nonsynonymous_SNV1	62847292	62847292	G	C	hom	164
Tvp23b	nonsynonymous_SNV1	62881943	62881943	A	C	hom	154
Myh8	nonsynonymous_SNV1	67289653	67289653	A	G	hom	222
Glp2r	nonsynonymous_SNV8	67709568	67709568	C	A	hom	186
Rnf222	nonsynonymous_SNV1	68893019	68893019	A	T	hom	165
Aurkb	nonsynonymous_SNV1	69047870	69047870	T	C	hom	184
Per1;Per1	nonsynonymous_SNV1	69108510	69108510	C	T	hom	222
Hes7	nonsynonymous_SNV1	69122956	69122956	T	C	hom	33
Aloxe3	nonsynonymous_SNV1	69128675	69128675	A	G	hom	222
Aloxe3	nonsynonymous_SNV1	69134001	69134001	G	A	hom	211
Chd3	nonsynonymous_SNV1	69361451	69361451	A	G	hom	221
Cyb5d1	nonsynonymous_SNV1	69395202	69395202	A	G	hom	148
Cyb5d1	nonsynonymous_SNV1	69395272	69395272	C	A	hom	164
Tmem102	nonsynonymous_SNV1	69805101	69805101	G	C	hom	140
Nlgn2	nonsynonymous_SNV1	69828394	69828394	A	G	hom	187
Kif1c	nonsynonymous_SNV1	70724114	70724114	C	T	hom	172
			Frameshift, stopgain				
Fat2	frameshift_deletion	55308977	55308989	CACCCCAGTACCT	-	hom	214
Olfr332	stopgain_SNV	58489748	58489748	C	A	hom	82.1
Olfr331	nonframeshift_deletion	58502393	58502404	TGGTATGTGGAT	-	hom	55.5
Btnl10	stopgain_SNV	58926877	58926877	G	T	hom	222
Obscn	nonframeshift_insertion	59000527	59000527	-	TGG	hom	214
Iba57	frameshift_insertion	59161506	59161506	-	GA	hom	214
Olfr223	stopgain_SNV	59589685	59589685	G	A	hom	215
Olfr225	frameshift_insertion	59613118	59613118	-	T	hom	214
Olfr225	stopgain_SNV	59613206	59613206	C	T	hom	222
Olfr225	frameshift_insertion	59613903	59613903	-	T	hom	214

Myo15	nonframeshift_deletion	60504278	60504280	TAG	-	hom	214
Trim16	nonframeshift_insertion	62820695	62820695	-	AGA	hom	214

SNV: single nucleotide variant. SNP: single nucleotide polymorphism. The letter after SNV shows the number of SNV in the coding region of each gene.

500

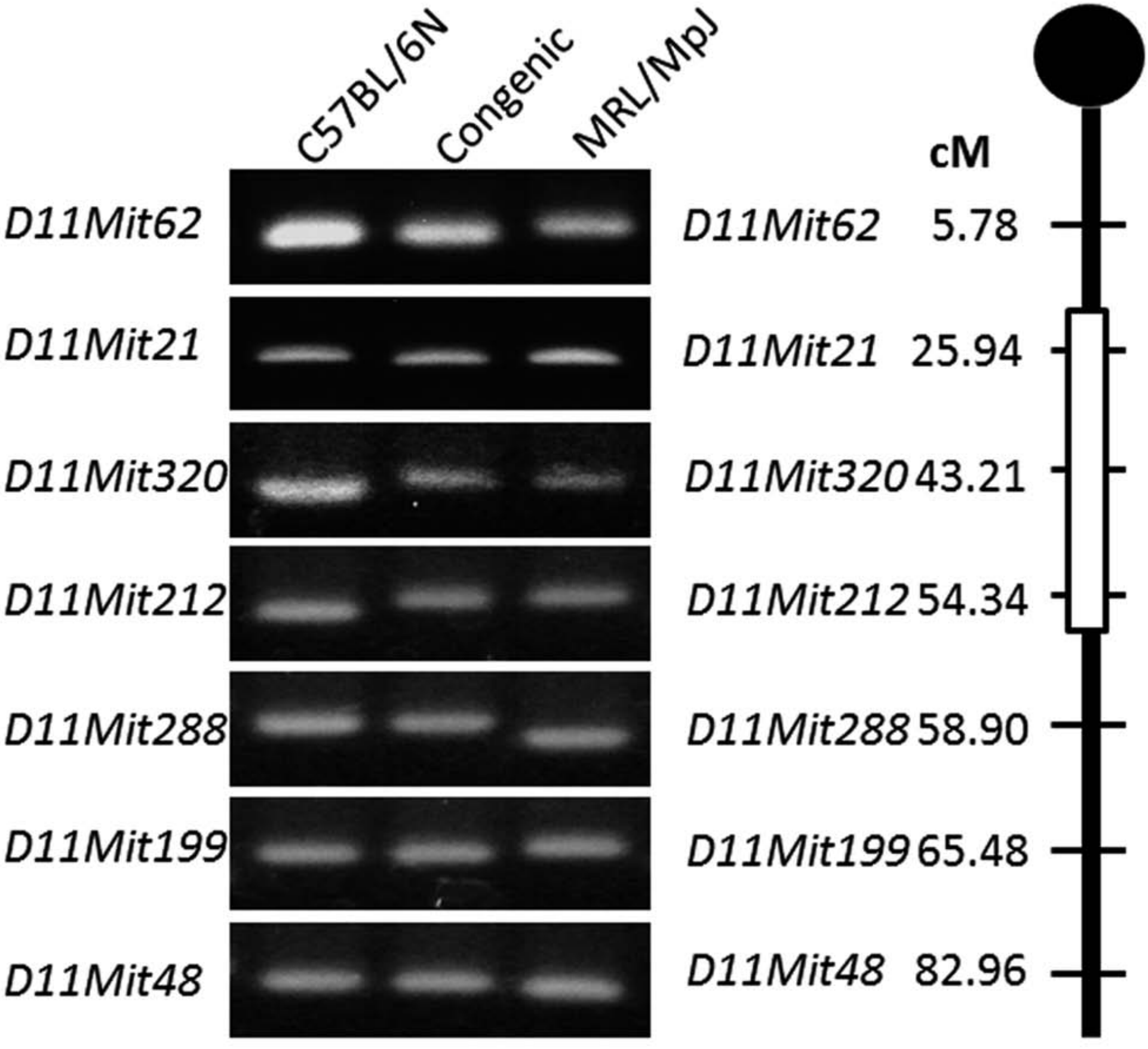
C57BL/6N
Congenic
MRL/MpJ
cM
D11Mit62
D11Mit21
D11Mit320
D11Mit212
D11Mit288
D11Mit199
D11Mit48
D11Mit62 5.78
D11Mit21 25.94
D11Mit320 43.21
D11Mit212 54.34
D11Mit288 58.90
D11Mit199 65.48
D11Mit48 82.96

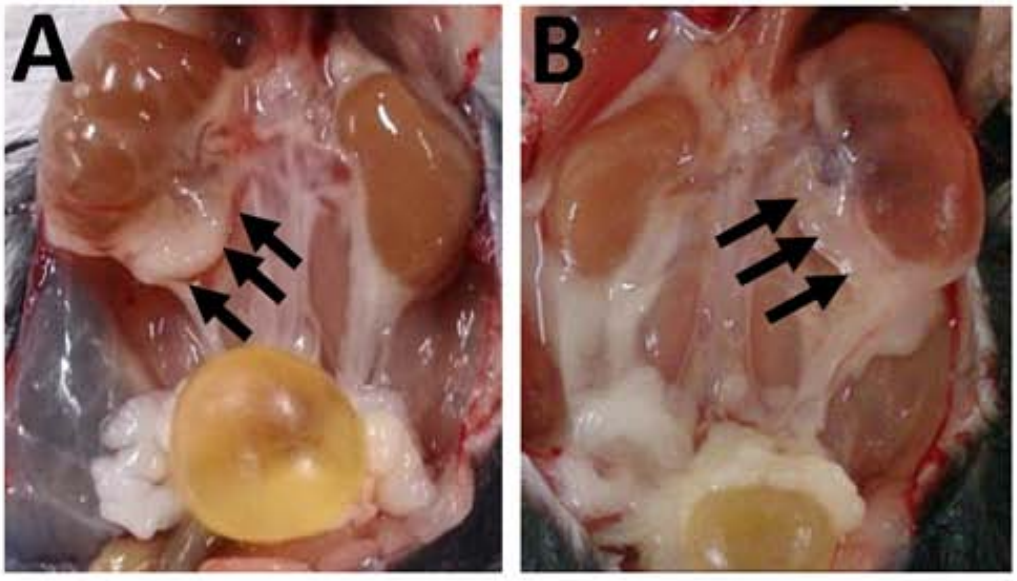
A
B

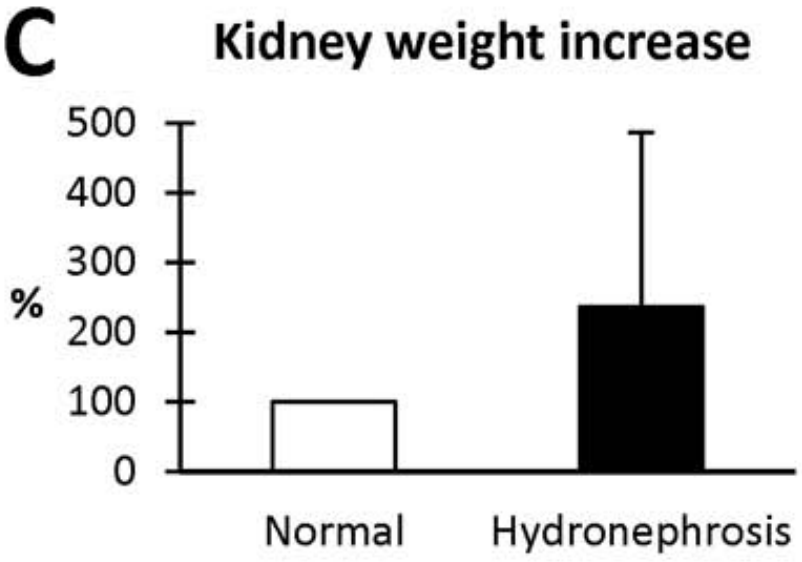
C
Kidney weight increase
500
400
300
%
200
100
0
Normal
Hydronephrosis

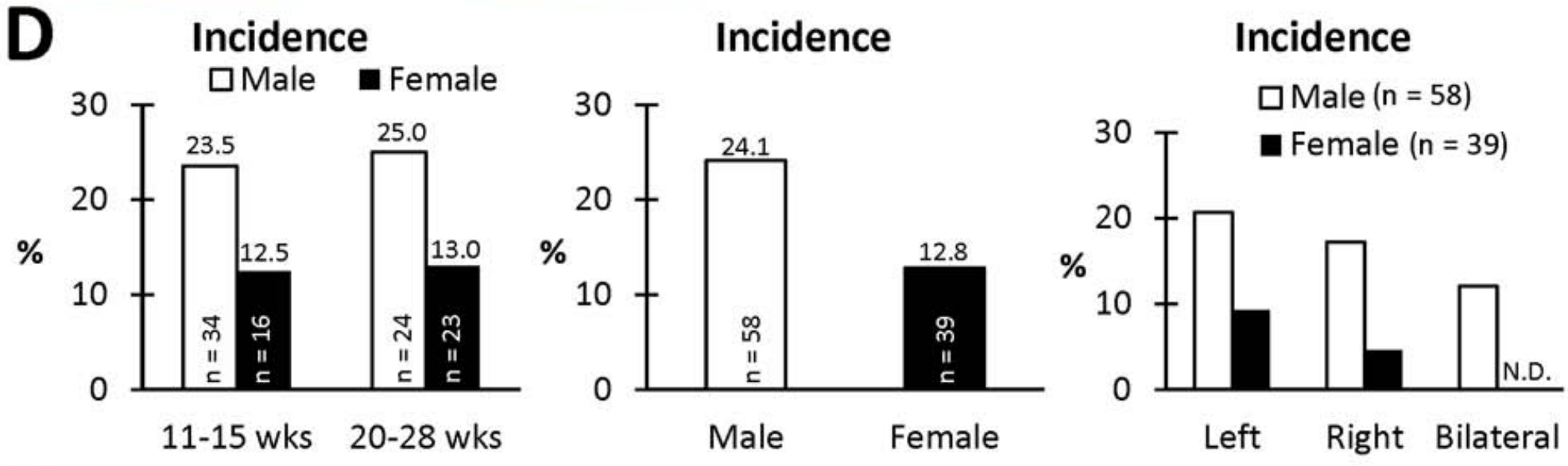
D
Incidence
Male
Female
30
20
%
10
0
23.5
12.5
25.0
13.0
n = 34
n = 16
n = 24
n = 23
11-15 wks
20-28 wks
Incidence
24.1
12.8
n = 58
n = 39
Male
Female
Incidence
Male (n = 58)
Female (n = 39)
N.D.
Left
Right
Bilateral

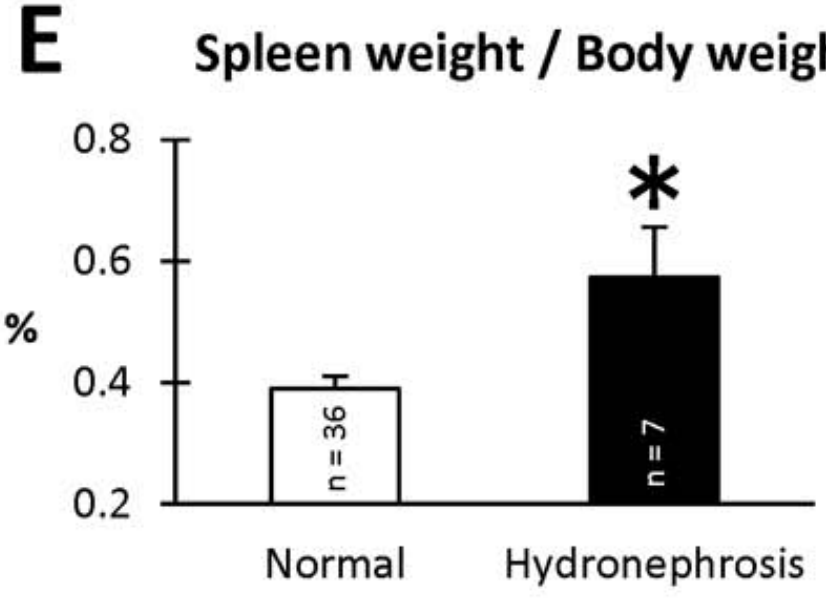
E
Spleen weight / Body weight
0.8
0.6
%
0.4
0.2
*
n = 36
n = 7
Normal
Hydronephrosis

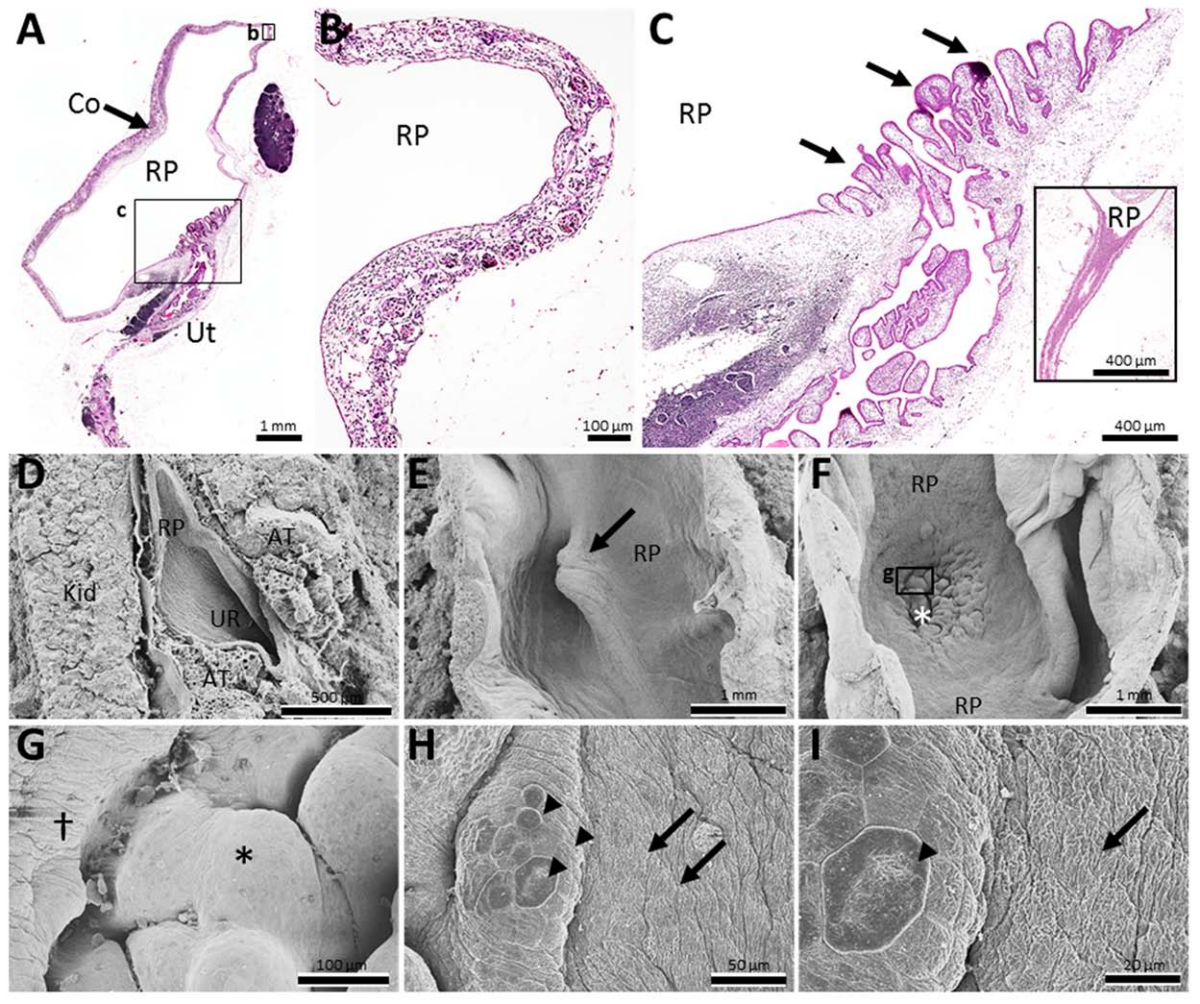
A
b
Co
RP
c
Ut
1 mm
B
RP
100 µm
C
RP
RP
400 µm
400 µm
D
RP
AT
Kid
UR
AT
500 µm
E
RP
1 mm
F
RP
g
RP
1 mm
G
†
*
100 µm
H
50 µm
I
20 µm

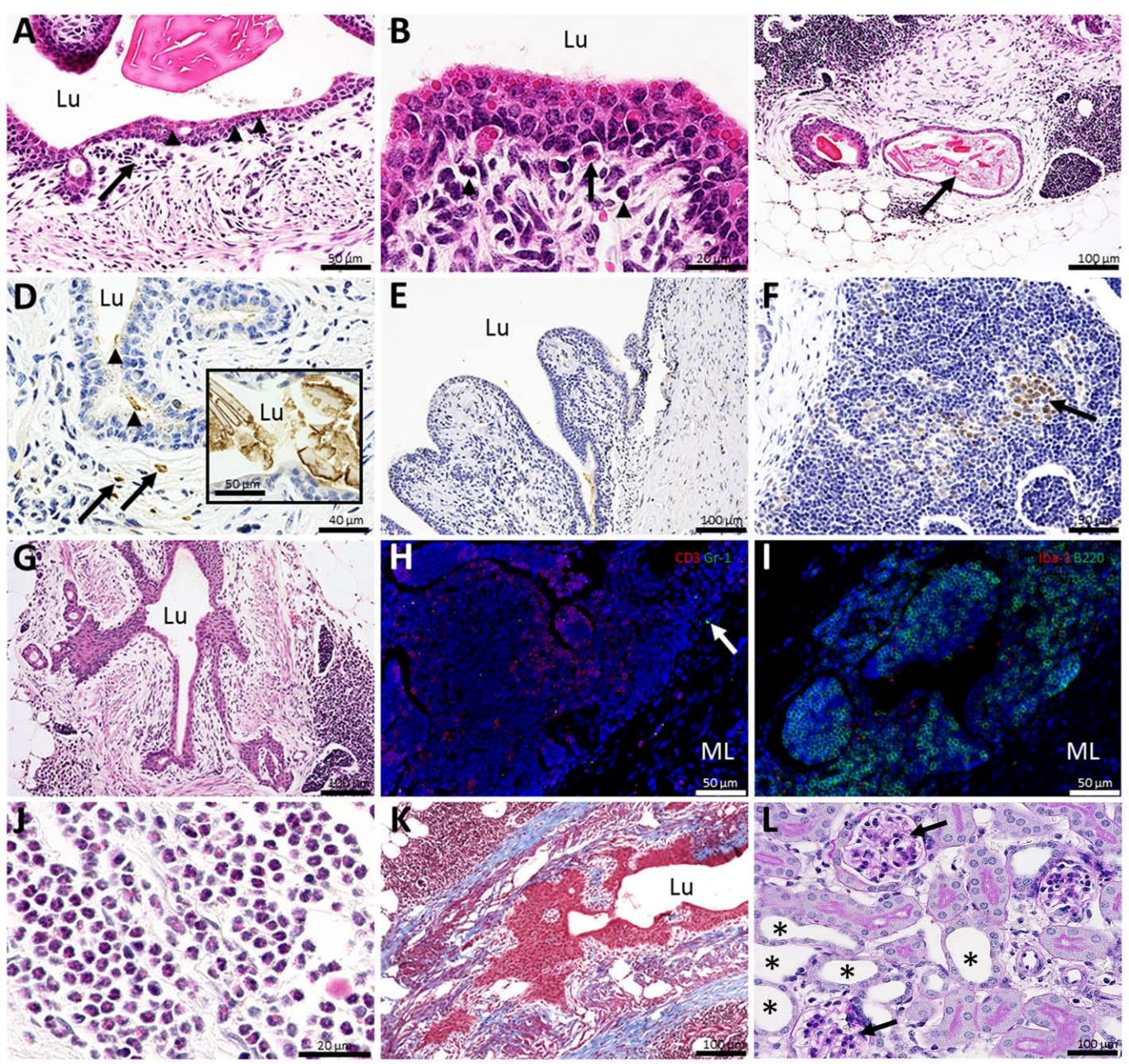
A
Lu
50 μm
B
Lu
20 μm
C
100 μm
D
Lu
Lu
50 μm
40 μm
E
Lu
100 μm
F
50 μm
G
Lu
100 μm
H
CD3 Gr-1
ML
50 μm
I
Iba-1 B220
ML
50 μm
J
20 μm
K
Lu
100 μm
L
100 μm

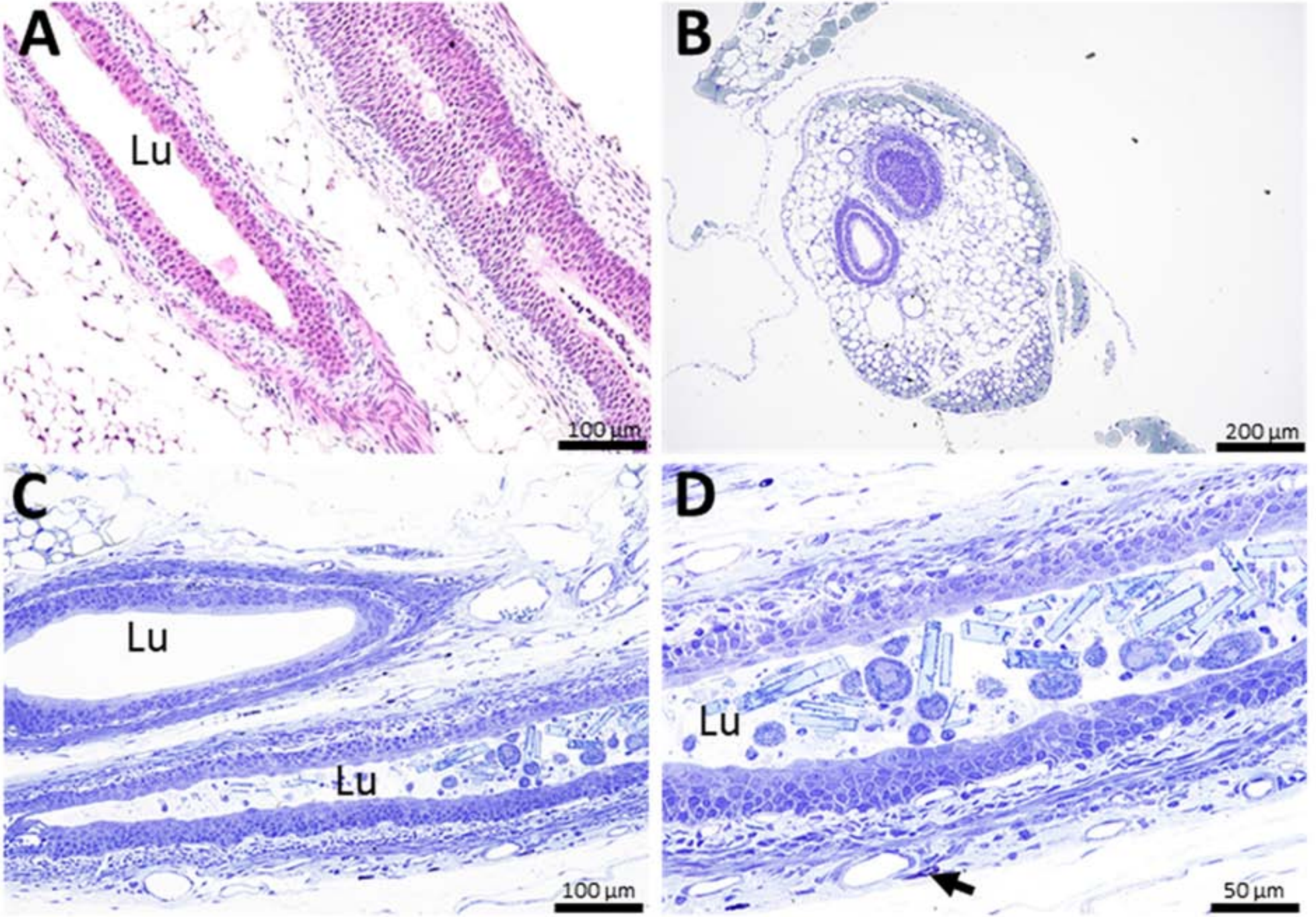
A
Lu
100 µm
B
200 µm
C
Lu
Lu
100 µm
D
Lu
50 µm